LRP 495/94 May 1994

GYROKINETIC APPROACH TO THE PROPAGATION OF ELECTROMAGNETIC WAVES IN NONUNIFORM BOUNDED PLASMA SLABS

O. Sauter & J. Vaclavik

This paper is accepted for publication in the 25th Anniversary Issue of Computer Physics Communication, which will be published mid-1994

Gyrokinetic approach to the propagation of electromagnetic waves in nonuniform bounded plasma slabs

O. Sauter and J. Vaclavik

Centre de Recherches en Physique des Plasmas
Associations Euratom - Confédération Suisse
Ecole Polytechnique Fédérale de Lausanne
21 Av. des Bains - CH-1007 Lausanne - Switzerland

A new code, SEMAL [1], has been developed which solves the linearized Vlasov-Maxwell wave equations to all orders in Larmor radii. Arbitrary density and temperature profiles as well as nonuniform magnetic fields are considered in slab geometry. The vacuum regions adjacent to the plasma slab are limited by perfectly conducting walls and contain an antenna as an excitation source. The linear response is obtained by solving the system of one first-order and two second-order integro-differential equations using a non-polluting finite element discretization. The general equations in the Fourier space, derived in a new comprehensive way, and their inverse transform, using $k_y = 0$, are described as well as the convergence and non-polluting properties of the method. We present the results concerning the influence of alpha particles on ICRF heating schemes for ITER, where we show that small alphas concentration can alter the steady-state operation envisaged with ICRF fast wave current-drive.

1. Introduction

Heating of tokamak plasmas and non-inductive current drive obtained with RF waves is one of the main subjects in plasma physics research. Much experimental and theoretical effort has been, and still is, devoted to the improvement of the heating efficiency and to the understanding of the wave-particle interactions. Many models describing the linear wave-particle interactions already exist, allowing one to analyse the absorption of the waves by the electrons and/or the ions. They can be separated into two main classes: ray-tracing models [2] and global wave models [3]. The latter describe the global wave field (sum of incident, transmitted and reflected fields) taking into account the finiteness of the plasma, the boundary conditions at the plasma-vacuum interfaces and the antenna. With this global wave approach, one is able to study scenarii where cut-off, reflected, resonant, mode converted and/or evanescent wave fields are present.

The most advanced global wave models are the "local" models which use a second-order expansion in $k_\perp \rho_\sigma$, where $k_\perp$ is the perpendicular wavenumber and ρ_σ the Larmor radius of species σ [4-8]. In this way, one obtains a system of three second-order differential equations [9]. However, the local models are limited to Larmor radii small compared with the wavelength or with the characteristic length of the density and temperature profiles. Moreover, they are limited to frequencies up to the second harmonic of the cyclotron frequency.

In present day experiments, and especially in the new generation of tokamaks where alpha particles are present, the temperature is very high. Moreover, many experiments use heating scenarii at high harmonic frequencies. Note that if alpha particles are present and second harmonic heating is considered, than the third harmonic of the alpha particles will be dominant in all the outer part of the plasma [10]. Moreover, for reactor-like parameters, one cannot model scenarii at the fundamental frequency of hydrogen, $f=f_H$, since the third harmonic of tritium is also in the plasma and modifies the dispersion relation. Because these cases can no longer be studied using these models, we have developed a gyrokinetic model for linear wave-particle interactions which is not limited to either the size of the Larmor radii

or the harmonic considered. This model is based on the global wave approach and can therefore treat the variety of problems mentioned above. The differential equations for the electric field are now replaced by one first-order and two second-order integro-differential equations. Nevertheless, we had to limit our work to uni-dimensional geometry, Maxwellian equilibrium distribution functions and slowly-varying equilibrium magnetic fields. We have also neglected k_y in the conductivity tensor, where y is in the direction normal to the direction of the inhomogeneity, along x, and to the magnetostatic field, along z. As we solve the equations in slab geometry, this new code SEMAL is a complement to the 2-D codes using second-order in Larmor radii expansion [5-8] or to a 2-D ray-tracing model valid to all orders in Larmor radii [11]. This gyrokinetic model was first used for electrostatic waves [12] and is now extended to electromagnetic (E.M.) waves.

In Section II, starting from the linearized Vlasov-Maxwell equations, we derive the equations in Fourier space, which we are able to write in a new comprehensive way including temperature gradients, and in the configuration space. We also derive a formula for the local power absorption, valid for this gyrokinetic model, allowing us to determine the absorption profile of the waves by the particles. The numerical method, finite element, is described in Section III, including the boundary conditions and the convergence and non-polluting properties of the code. We show the effect of alpha-particles on ICRF heating for a broad range of ITER scenarii in Section IV, and we conclude in Section V.

2. Physics Problem

We start from the linearized Vlasov-Maxwell system of equations, assuming $|f_\sigma^{(1)}| << f_\sigma^{(0)}$, $\mathbf{E} = \mathbf{E}^{(1)}$, $|\mathbf{B}^{(1)}| << |\mathbf{B}_0|$ and $\mathbf{j} = \mathbf{j}^{(1)}$:

$$\mathbf{v}\cdot\nabla f_\sigma^{(0)} + \frac{q_\sigma}{m_\sigma}\mathbf{v}\times\mathbf{B}_0 \cdot\frac{\partial}{\partial \mathbf{v}} f_\sigma^{(0)} = 0 \ , \tag{1a}$$

$$\left(\frac{\partial}{\partial t} + \mathbf{v}\cdot\nabla\right) f_\sigma^{(1)} + \frac{q_\sigma}{m_\sigma}\mathbf{v}\wedge\mathbf{B}_0 \cdot\frac{\partial}{\partial \mathbf{v}} f_\sigma^{(1)} = -\frac{q_\sigma}{m_\sigma}\left(\mathbf{E}^{(1)} + \mathbf{v}\wedge\mathbf{B}^{(1)}\right)\cdot\frac{\partial}{\partial \mathbf{v}} f_\sigma^{(0)} \ , \tag{1b}$$

$$\nabla \times \mathbf{E}^{(1)} = -\frac{\partial \mathbf{B}^{(1)}}{\partial t} \quad , \tag{1c}$$

$$\nabla \times \mathbf{B}^{(1)} = \mu_0 \mathbf{j}^{(1)} + \frac{1}{c^2}\frac{\partial \mathbf{E}^{(1)}}{\partial t} , \tag{1d}$$

$$\mathbf{j}^{(1)} = \sum_{\sigma} q_\sigma \int \mathbf{v} f_\sigma^{(1)}(\mathbf{r}, \mathbf{v}, t)\, d^3\mathbf{v} , \tag{1e}$$

where f_σ is the distribution function of species σ, $\mathbf{E}^{(1)}$ and $\mathbf{B}^{(1)}$ the E.M. wave fields, $\mathbf{B}_0$ the equilibrium "toroidal" magnetic field parallel to the z axis, and $\mathbf{j}^{(1)}$, the perturbed current. These are the equations which determine the self-consistent linear response of the particles due to a small external R.F. perturbation. We seek oscillatory solutions due to this perturbation proportional to $e^{i(k_{||}z-\omega t)}$, where $k_{||}$, determined by the antenna, is the wavenumber parallel to $\mathbf{B}_0$, and ω is the frequency of the antenna current. In order to satisfy the causality condition, ω is assumed to have a small positive imaginary part.

2.1 k-space integral equation

Taking the Fourier transform of Eq.(1) and assuming, for simplicity, a uniform magnetic field, we can solve Eq.(1b), using Eqs.(1a) and (1c), and obtain $f_\sigma^{(1)}(\mathbf{k}, \mathbf{v})$ in terms of $f_\sigma^{(0)}$, $\mathbf{B}_0$ and $\mathbf{E}^{(1)}$ [13]. We then have to specify the velocity dependence of $f_\sigma^{(0)}(\mathbf{k}, \mathbf{v})$, which we assume bi-Maxwellian, and we use the slab geometry to specify that the density and temperature profiles are inhomogeneous only in the x direction. Thus we have

$$f_\sigma^{(0)}(\mathbf{k}_\perp, v_\perp, v_{//}) = f_\sigma^{(0)}(k_x, v_\perp, v_{//}) = \frac{1}{2\pi^{5/2}} \int dx'' \, \frac{n_\sigma(x'')}{v_{T\sigma\perp}^2(x'')\, v_{T\sigma//}(x'')} \times \exp\left\{-\frac{v_\perp^2}{v_{T\sigma\perp}^2(x'')} - \frac{v_{//}^2}{v_{T\sigma//}^2(x'')}\right\} e^{-i k_x x''} , \tag{2}$$

where $\mathbf{k}_\perp = (k_x, k_y)$ and $n_\sigma(x'')$, $v^2_{T\sigma}(x'') = 2T_\sigma(x'')/m_\sigma$ are the density and thermal velocity squared of the guiding centres of species σ respectively. We shall always use x'' as the variable for the guiding centre coordinate.

Introducing $f^{(1)}_\sigma(\mathbf{k}, \mathbf{v})$ into Eq.(1e) and $\mathbf{j}^{(1)}$ into Eq.(1d), and integrating over velocity, we obtain the integral equation in the Fourier space for the perturbed electric field $\mathbf{E}(\mathbf{k})$ of the form:

$$\mathbf{k} \wedge \mathbf{k} \wedge \mathbf{E}(\mathbf{k}) + \frac{\omega^2}{c^2} (\underline{\underline{\varepsilon}}\mathbf{E})(\mathbf{k}) = 0, \tag{3}$$

with

$$(\underline{\underline{\varepsilon}}\mathbf{E})(\mathbf{k}) = \underline{\underline{I}}\mathbf{E}(\mathbf{k}) + \int dk'_x \, \underline{\underline{K}}(\mathbf{k}, \mathbf{k}') \, \mathbf{E}(\mathbf{k}'), \tag{4}$$

where $\mathbf{k} = (k_x, k_y, k_{//})$, $\mathbf{k}' = (k'_x, k_y, k_{//})$, and $\underline{\underline{I}}$ is the identity tensor. Before writing explicitly the kernel tensor $\underline{\underline{K}}$, we need to introduce the angle ψ between $\mathbf{k}_\perp$ and $\mathbf{k}'_\perp$, in the same way as Watanabe et al. [14], except for the sign:

$$\tan\psi = \frac{(\mathbf{k}_\perp \wedge \mathbf{k}'_\perp)_{//}}{\mathbf{k}_\perp \cdot \mathbf{k}'_\perp} = \frac{(k_x - k'_x) k_y}{k_x k'_x + k_y^2}.$$

Note also that the integral over $v_\parallel$ is performed using the plasma dispersion function as defined by Fried and Conte [15]: $Z[\xi_{n\sigma} = (\omega - n\omega_{c\sigma})/|k_{//}| v_{T\sigma//}]$. Equation (4) then reads [1]:

$$(\underline{\underline{\varepsilon}}\mathbf{E})(\mathbf{k}) = \underline{\underline{I}}\mathbf{E}(\mathbf{k}) + \sum_{\sigma,n} \int dx'' \, dk'_x \, \frac{\omega^2_{p\sigma}(x'')}{2\pi\omega^2} e^{-i(k_x - k'_x)x''} e^{-\frac{1}{2}(\beta - \beta')} e^{in\psi}$$

$$\times \left\{ \left[\frac{\omega - i\omega^*_\sigma}{|k_{//}| v_{T\sigma//}} Z(\xi_{n\sigma}) - (1 + \xi_{n\sigma} Z(\xi_{n\sigma}))\left(1 - \frac{T_{\sigma\perp}}{T_{\sigma//}}\right) \right] \underline{\underline{M}} + \delta^{Kr.}_{0n} \, \underline{\underline{D}} \, e^{z\cos\psi} \right\} \mathbf{E}(\mathbf{k}', \omega), \tag{5}$$

with

$$M_{xx}(k_x,k'_x) = [\frac{n^2}{z}\cos\psi + 2k_y^2\rho_\sigma^2 - i\frac{n}{z}(k_xk'_x - k_y^2)\rho_\sigma^2\sin\psi\,]\,I_n$$

$$- [\,in\sin\psi + \frac{k_y^2\rho_\sigma^2}{z}(\beta+\beta')\,]\,\Gamma_n\,,$$

$$M_{yy}(k_x,k'_x) = [\frac{n^2}{z}\cos\psi + 2k_xk'_x\rho_\sigma^2 + i\frac{n}{z^2}(k_x\beta - k'_x\beta')\,k_y\rho_\sigma^2\,]\,I_n$$

$$- [\,in\sin\psi + \frac{k_xk'_x\rho_\sigma^2}{z}(\beta+\beta')\,]\,\Gamma_n\,,$$

$$M_{zz}(k_x,k'_x) = \Xi_{n\sigma}^2\,I_n\,,$$

$$M_{xy}(k_x,k'_x) = [\frac{n^2}{z}\sin\psi + 2k_yk'_x\rho_\sigma^2 - i\frac{n}{z^2}(k_y^2\beta + k_xk'_x\beta')\,\rho_\sigma^2\,]\,I_n$$

$$+ [\,in\cos\psi + \frac{k_yk'_x\rho_\sigma^2}{z}(\beta+\beta')\,]\,\Gamma_n\,,$$

$$M_{xz}(k_x,k'_x) = \Xi_{n\sigma}\,\{[\frac{n}{z^2}k_x\rho_\sigma\beta' - ik_y\rho_\sigma\,]\,I_n + i\frac{k_y\rho_\sigma}{z}\beta'\,\Gamma_n\}\,,$$

$$M_{yz}(k_x,k'_x) = \Xi_{n\sigma}\,\{[\frac{n}{z^2}k_y\rho_\sigma\beta' + ik_x\rho_\sigma\,]\,I_n - i\frac{k_x\rho_\sigma}{z}\beta'\,\Gamma_n\}\,,$$

$$M_{ij}(k_x,k'_x) = M_{ji}^*(k'_x,k_x)\quad,$$

and

$$\underline{\underline{D}} = \begin{pmatrix} 0 & 0 & 0 \\ 0 & -(k_x-k'_x)^2\rho_\sigma^2 & -i\,(k_x-k'_x)\dfrac{\omega - i\omega_\sigma^*}{k_{//}\,\omega_{c\sigma}} \\ 0 & D_{yz} & \dfrac{(\omega - i\omega_\sigma^*)^2}{(k_{//}\,v_{T\sigma//})^2}\,\dfrac{2T_{\sigma//}}{T_{\sigma\perp}} \end{pmatrix}, \qquad (6)$$

where

$$\Xi_{n\sigma} = \frac{\omega - n\omega_{c\sigma}}{k_{//}\,\omega_{c\sigma}}\,\frac{1}{\rho_\sigma}\,,$$

$$\omega^*_\sigma = \omega_{c\sigma}\,k_y\,(k_x - k'_x)\,\rho^2_\sigma\,,$$

$$I_n = I_n(z)\quad,\quad z = k_\perp\,k'_\perp\,\rho^2_\sigma\quad,\quad \beta = k^2_\perp\,\rho^2_\sigma\quad,\quad \beta' = k'^2_\perp\,\rho^2_\sigma\,,$$

$$\omega^2_{p\sigma} = \frac{n_\sigma q^2_\sigma}{\varepsilon_0\,m_\sigma}\quad,\quad v^2_{T\sigma(\perp,//)} = \frac{2\,T_{\sigma(\perp,//)}}{m_\sigma}\quad,\quad \rho_\sigma = \frac{v_{T\sigma\perp}}{\sqrt{2}\,|\omega_{c\sigma}|}\,,$$

and where $\omega_\sigma = q_\sigma B_0/m_\sigma$ is the cyclotron frequency, $\omega_{p\sigma}$ the plasma frequency, I_n the modified Bessel function and n the harmonic number. The dielectric tensor $(\underline{\underline{\varepsilon}}\mathbf{E})(\mathbf{k})$, which is an integral operator, has been checked with the one obtained in Ref. [14] assuming a Gaussian density profile and uniform temperature profiles. Watanabe et al. [14] were the first to derive this equation, followed by others [16, 17] who assumed arbitrary density profiles. The integral equations derived here, Eqs.(3) and (5), are generalizing these results to arbitrary temperature profiles. Moreover, we have summed over n some terms independent of the plasma dispersion function Z (non-resonant terms) using

$$\sum_n \cos n\psi\; I_n(z) = e^{z\cos\psi}\,, \tag{7}$$

and introduced these terms into the tensor $\underline{\underline{D}}$ (Eq.(6)). In this way, we are able to define the same matrix $\underline{\underline{M}}$ for isotropic and anisotropic distributions, and our equations are written in a much more compact and comprehensive way than in Refs. [14, 16, 17]. Note also that as $\underline{\underline{M}}(k_x, k'_x)$ and $\underline{\underline{D}}(k_x, k'_x)$ are Hermitian and as $i\omega^*_\sigma(k'_x, k_x) = -i\omega^*_\sigma(k_x, k'_x)$, we see from Eq.(5) that $(\underline{\underline{\varepsilon}}\mathbf{E})$ is Hermitian if we assume no dissipation ($Z_{n\sigma}$ real). The dispersion relation is obtained assuming an infinite homogeneous plasma and integrating over k'_x in Eq.(5). It is described in Ref. [1] as well as the code DISPAL solving the real part of the

dispersion relation obtained from Eq.(5). Note, nevertheless, that the dispersion relation is exact in the sense that it has only physical roots and no extra spurious roots which might appear when an expansion in $k_\perp \rho_\sigma$ is used.

2.2 Equation in configuration space

Using an integral representation for the modified Bessel function I_n:

$$I_n(z) = \frac{1}{\pi}\int_0^\pi e^{z\cos\theta}\cos(n\theta)\,d\theta \quad , \tag{9}$$

we are able to calculate analytically the inversion integrals. However, we first need to neglect k_y in the dielectric tensor $\underline{\underline{\varepsilon}}$, which corresponds to assuming $\omega_\sigma^* << \omega$ and is valid for studying all the frequencies between Alfvén and electron cyclotron. In this way, we obtain the equation for the three components of the electric field **E** in slab geometry, valid for arbitrary density and temperature profiles, and slowly varying magnetic fields, $k_{//}R_0 >> \sqrt{T_\perp/T_{//}}$ (R_0 being the major radius), assuming bi-Maxwellian distribution functions and $k_y = 0$ [1]:

$$\nabla\wedge\nabla\wedge\mathbf{E}(x) - \frac{\omega^2}{c^2}\,(\underline{\underline{\varepsilon}}\,\mathbf{E})(x) = 0\,, \tag{10}$$

where $\nabla = (\frac{d}{dx}, ik_y, ik_z)$ and with

$$(\underline{\underline{\varepsilon}}\,\mathbf{E})(x) = \underline{\underline{I}}\,\mathbf{E}(x) + \sum_\sigma \int dx''\,\frac{\omega_{p\sigma}^2(x'')}{\sqrt{2\pi}\,\omega^2\rho_\sigma}\exp\left[-\frac{(x-x'')^2}{2\rho_\sigma^2}\right]\underline{\underline{D}}\,\mathbf{E}(x)$$

$$+\sum_{\sigma,n}\int dx''\,dx'\int_0^\pi d\theta\,\frac{\omega_{p\sigma}^2(x'')}{2\pi^2\omega^2\rho_\sigma^2(x'')}\exp\left\{-\frac{(x''-\frac{x+x'}{2})^2(1-\cos\theta)}{\rho_\sigma^2(x'')\sin^2\theta}\right\}$$

$$\times\exp\left\{-\frac{(x-x')^2(1+\cos\theta)}{4\rho_\sigma^2(x'')\sin^2\theta}\right\}\left[\frac{\omega}{|k_{//}|v_{T\sigma//}}Z_{n\sigma} - (1+\xi_{n\sigma}Z_{n\sigma})(1-\frac{T_{\sigma\perp}}{T_{\sigma//}})\right]\underline{\underline{M}}\,\mathbf{E}(x')$$

and

$$\underline{\underline{M}} = \begin{pmatrix} n \sin n\theta & -i\frac{\sin n\theta}{\sin^2\theta}\frac{(x'-x'')}{\rho_\sigma^2}\times & i\frac{\sin n\theta}{\sin^2\theta}\Xi_{n\sigma}\times \\ & \times[(x-x'')\cos\theta-(x'-x'')] & \times\frac{[(x-x'')\cos\theta-(x'-x'')]}{\rho_\sigma} \\ M^*_{xy}(x',x) & \frac{\cos n\theta}{\sin\theta}\frac{(x-x'')(x'-x'')}{\rho_\sigma^2} & -\frac{\cos n\theta}{\sin\theta}\Xi_{n\sigma}\frac{(x-x'')}{\rho_\sigma} \\ M^*_{xz}(x',x) & M^*_{yz}(x',x) & \frac{\cos n\theta}{\sin\theta}\Xi^2_{n\sigma} \end{pmatrix},$$

$$\underline{\underline{D}} = \begin{pmatrix} 0 & 0 & 0 \\ 0 & -1+\frac{(x-x'')^2}{\rho_\sigma^2} & -\Xi_0\frac{(x-x'')}{\rho_\sigma} \\ 0 & D_{yz} & \Xi_0^2 \end{pmatrix}.$$

It should be pointed out that the appropriate derivation of Eq.(10) for a nonuniform magnetic field could follow a more complicated method used in Ref. [28]. If one then assumes $k_{//}R_0 >> \sqrt{T_\perp/T_{//}}$ one may evaluate the magnetic field at the position of the particle instead of its guiding centre and one obtains the same equation. Thus the effects neglected may be important only for very small $k_{//}$ scenarii, which are not considered in this study.

Assuming isotropic temperature, $T_\perp = T_{||}$, and including the terms D_{yz} and D_{zz} into M_{yz} and M_{zz} respectively, one recovers the formula published in Ref. [10]. Note however that even with $T_\perp = T_{||}$, the term D_{yy} is different from the M_{yy} term and represents an extra non-resonant term due to the inhomogeneity.

The system of equations for **E**, Eq.(10), consists of one first order and two second order integro-differential equations for E_x and E_y, E_z, respectively. This asymmetry between E_x and E_y, E_z, due to the slab geometry, requires a special finite element method in order to avoid pollution. This is discussed in Section III, together with the boundary conditions needed to close the system of equations.

2.3 Local power absorption formula

Following the procedure described in Ref. [18, 19] we obtain the following formula for the local power absorption $P_L(x)$ [20], generalized to anisotropic temperature and having the same domain of validity as Eq.(10). It is therefore consistent with the wave-field solution **E**(x):

$$P_L(x) = \sum_{n,\sigma} \frac{2q_\sigma^2}{\pi^{5/2} m_\sigma} \int dx'' \int_0^{\frac{\pi}{2}} d\theta \frac{n_\sigma(x'')}{|k_{//}| v_{T\sigma//}(x'')} \frac{\omega_{c\sigma}^4(x'')}{v_{T\sigma\perp}^4(x'')} \frac{|x - x''|^3}{\cos^4\theta}$$

$$\times e^{-\xi_{n\sigma}^2} \exp\left\{-\frac{(x - x'')^2}{2\rho_\sigma^2 \cos^2\theta}\right\} \frac{T_{\sigma\perp}}{T_{\sigma//}} \left[1 - \frac{n\omega_{c\sigma}}{\omega}\left(1 - \frac{T_{\sigma//}}{T_{\sigma\perp}}\right)\right] \qquad (12)$$

$$\times \left| \int_0^{\pi} d\theta' \left[E_x \sin\theta' \sin n\theta' + i \cos n\theta' \left(\cos\theta' E_y + \frac{(\omega - n\omega_{c\sigma})\cos\theta}{k_{//}\omega_{c\sigma}|x - x''|} E_{//}\right)\right] \right|^2 ,$$

with $\mathbf{E} = \mathbf{E}\left(x'' - \frac{|x - x''|}{\cos\theta}\cos\theta'\right)$. We see that $P_L(x)$ is positive-definite in the isotropic case, because we have assumed slowly varying magnetic fields and $k_y = 0$, and this is why we can call it the local power absorption, that is the absorption between x and x+dx. However $P_L(x)$ is nonlocal in the sense that it depends on the value of the field throughout the plasma, which is due to the gyrokinetic approach. The width of this nonlocal contribution is nevertheless limited by the term $\exp\{-(x-x'')^2/(2\rho_\sigma^2\cos^2\theta)\}$ to four or five Larmor radii. We see also that if $T_{\sigma\perp} > 2T_{\sigma||}$ and $\omega > \omega_{c\sigma}/2$, kinetic instabilities may exist in some special cases when

$$1 - \frac{n\omega_{c\sigma}}{\omega}\left(1 - \frac{T_{\sigma//}}{T_{\sigma\perp}}\right) < 0 ,$$

and if ω is not too far from a harmonic frequency [21]. Finally, note that only resonant particles, characterised by the term $\exp\{-\xi^2_{n\sigma}\}$, contribute to $P_L(x)$.

3. Numerical problem

3.1 Numerical scheme and pollution problems

We solve Eq.(10) using the finite element method with piece-wise constant basis functions for E_x and linear for E_y and E_z. This is to avoid pollution and we shall describe it briefly here.

In order to obtain the weak form of Eq.(10), we multiply it by a test function $G^*(x)$ and integrate over the x domain considered $[x_{pl}, x_{pr}]$, where x_{pl} and x_{pr} are the left and right plasma boundary respectively. We then discretize $[x_{pl}, x_{pr}]$ in N intervals of arbitrary length and approximate $\mathbf{E}(x)$ as follows:

$$\begin{aligned} E_x(x) &= \sum_{j=1}^{N} E_x^j \chi_j(x), \\ E_{y,z}(x) &= \sum_{j=1}^{N} E_{y,z}^j \varphi_j(x). \end{aligned} \tag{13}$$

where $\chi_j(x)$ is the basis function used for E_x and φ_j the one used for E_y and E_z. We allow for different basis functions for E_x and E_y, E_z, because the equation is itself of different order for E_x, first-order, and E_y, E_z, second-order. Note that the integral part of the equation can be discretized by piece-wise constant basis functions, however $\varphi_j(x)$ has to be at least of first order in x as the differential part of the equation is second-order for E_y, E_z. The simplest choice would be to use linear basis function for all three components. However, the dispersion relation of this discretized system for the $\nabla\wedge\nabla\wedge\mathbf{E} - (\omega^2/c^2)\mathbf{E}$ part of the equation is polluted as can be seen in Fig.1 [1]. Indeed, the branch labelled 2 has two roots for $\omega^2/k_z^2c^2 \sim 1.5$, and most important, the branch labelled 3 has a root for

$\omega < k_z c$ where none should exist. On the other hand, if one uses piece-wise constant for χ_j and linear for φ_j, then the dispersion relation has only one non-trivial root (twice degenerated), corresponding to the branch labelled 1 in Fig.1, which approximates correctly the exact dispersion relation $\omega^2 = (k^2 + k_z^2)c^2$. We have shown in Ref. [1] that the use of Hermite cubic basis functions for both χ_j and φ_j also leads to a polluted discretized system, and that one should use quadratic basis for χ_j and cubic for φ_j in order to avoid pollution. However in our case, we have chosen piece-wise constant for χ_j and linear for φ_j for simplicity and because much analytical work is still needed in order to obtain a good numerical scheme for solving Eq.(10), as will be discussed later.

3.2 Boundary conditions

There are many different possible boundary conditions and, in the framework of the finite element method, they can be easily introduced in the numerical scheme. The typical set-up of the physics problem is shown in Fig. 2, where the plasma is surrounded by vacuum and an infinitely thin current sheet represents the antenna. The walls are supposed to be perfectly conducting. The set-up is adequate to simulate waves launched by an antenna current in the ion-cyclotron range of frequency (ICRF). The antenna current is defined by:

$$\mathbf{j}_a = (J_y \mathbf{e}_y + J_z \mathbf{e}_z)\, \delta(x - x_a)\,, \tag{14}$$

with $k_y J_y + k_z J_z = 0$, assuming $\nabla \cdot \mathbf{j}_a = 0$, $\mathbf{j}_a \approx \exp\{i(k_y y + k_z z - \omega t)\}$, and $\delta(x-x_a)$ is the Dirac distribution. The Maxwell equations in vacuum are solved analytically following Ref.[22] such as to provide the value of B_y and B_z at x_{pl} and x_{pr}, as a function of the antenna parameters, as boundary conditions for Eq.(10). Then, once Eq.(10) is solved, we can use the value of $E_y(x_{pr})$ and $E_z(x_{pr})$ to calculate the power P_a emitted by the antenna [22].

Another set of boundary conditions consists of directly imposing E_y, E_z at the plasma edges, simulating the electric field generated by a wave-guide. These boundary conditions were used in particular for studying the coupling between a wave-guide and the ion Bernstein wave in the FTU tokamak (Frascati tokamak upgrade, Italy) [24, 1].

3.3 Numerical integration of the kernel

To construct the weak form, we assume the test function $\eta_i^v(x)$ and introduce Eq.(13). The integral part contribution of the weak form is then

$$\sum_{w=x,y,z} \sum_{j=1}^{N} \int_{x_{i-1}}^{x_{i+1}} dx\, \eta_i^v(x) \int_{x_{j-1}}^{x_{j+1}} dx'\, K_{vw}(x,x')\, \eta_j^w(x') \,, \qquad \text{for } i=1,\cdots,N\,;\, v=x,y,z\,, \tag{15}$$

where

$$\eta_m^t(x) = \begin{cases} \chi_m(x) \,, & \text{for } t = x\,, \\ \varphi_m(x) \,, & \text{for } t = y \text{ and } z\,. \end{cases}$$

In general, we use Gaussian quadrature to calculate the different integrals involved in the weak form. However, integrand of the kernel of Eq.(10) is singular near $\bar{\theta} = 0$, $x = x'$ and $\bar{\theta} = \pi$, $x'' = (x-x')/2$. We have shown in Ref. [1], by performing a change of variable for x'' and x', that this $1/(\theta-\bar{\theta})$ singularity of the integrand disappears and is replaced by limits of integration proportional to $1/(\theta-\bar{\theta})$ at the singular points. However, due to the exponential terms in the integrand, the integral is finite showing that the singularity is integrable. Nevertheless, it is not integrable numerically as it stands and performing these changes of variables modifies the limits of integration for x'' and x', such that they depend on the other variables, which is very slow to compute. Therefore we have chosen another method to regularize the kernel integral and which also saves computing-time. We integrate analytically the kernel

contribution to the weak form, Eq.(15), over x and x'. It is possible to perform exact integration over x, x' because K(x,x') is proportional to exp{g(x,x')}, where g is a polynominal of second order in x, x'. However, this analytical integration requires the explicit form of the basis functions η^t_m in Eq.(15), and therefore reduces the flexibility of changing the numerical scheme by easily changing the basis functions, as is usually the case in finite element methods. This also explains why we have chosen piece-wise constant and linear basis functions instead of quadratic and cubics. Note that error functions have now to be evaluated, but this does not alter the vectorizability and speed of the scheme, as we use a rational approximation for the error function [23, formula 7.1.25]. Finally, the x" points are very much related to x, x' and (x+x')/2, therefore one has to use x and x" meshes as uniform with respect to one another as possible. Typically we choose NXPP=NX or NXPP=NX/2. We also note that we have to construct and solve a full matrix system. However, due to the exponential terms in K(x,x'), the contribution of the off-diagonal points decreases rapidly and can be neglected at typically $|x-x'| \leq 10\rho_\sigma$. This reduces considerably the CPU time needed to solve Eq.(10). Nevertheless, when alpha particles are present, their Larmor radius is around 4-5 cm, which means that they contribute over a range of about ±50 cm.

3.4 Convergence properties and comparison with the code ISMENE

We have studied the convergence properties of the code SEMAL in the Alfvén wave range of frequencies (AWRF). The plasma parameters are the following: $B_0 = 1T$, $n_e = n_D = 10^{19}m^{-3}$, Te = 1keV, T_D = 10 eV, $k_y = 0$, $k_z = 3m^{-1}$, $\omega/\omega_{cD} = 0.298$. The density and temperature profiles are parabolic, B_0 uniform and the antenna current is purely poloidal ($J_z = 0$). The ion temperature is taken very low to make sure that $k_\perp\rho_\sigma << 1$ enabling us to compare our gyrokinetic model with a local model, solving the equations expanded up to second-order in Larmor radii, code ISMENE [4]. In Fig.3 we show the convergence study of the real and imaginary parts of $E_x(x_{pr})$ versus $1/NX^2$, where NX is the number of mesh points. Other quantities, like the real part of

the power emitted by the antenna P_a, do not converge as well as E_x, however the relative error between coarse and fine grids stays within 1% [1].

In Fig.4, we compare the results obtained with SEMAL and ISMENE in the AWRF. We see that they match very well, as expected since we have chosen $k_\perp \rho_\sigma << 1$. The different peaks in P_a are due to the kinetic Alfvén wave (KAW), around $\omega/\omega_{ci} = 0.3$, and to the surface mode of the fast magnetosonic wave (large peak).

This shows that SEMAL converges and gives the correct results. Moreover we always check that the wave-field solution obtained with SEMAL is consistent with the dispersion relation obtained from Eqs.(3) and (5).

4. Effects of alpha particles on ICRF scenarii for ITER

We study the effects of α-particles on ICRF scenarii for ITER, based on the plasma parameters discussed at the ITER Technical Meeting on RF Heating and Current Drive [25]. Considering the broad-band antenna proposed at the meeting, we use the following parameters:

$$f = 20 - 90 \text{ MHz},$$
$$B_0 = 2 - 6 \text{ T},$$
$$n_{//} = k_{//}\, c / \omega = 2 - 10,$$
$$n_\alpha / n_e = 0 - 10\%,$$

where the ion species are D, T, alphas and eventually He^3 or H, and the fixed parameters are: R_0=7.7 m, a=2.8 m, k_y=1 m^{-1}, n_D/n_T=1 (except for f=43MHz), $n_e=10^{20}$ m^{-3}, $n_e=\Sigma\, Z_i n_i$, $T_e=T_{ions}$=25 keV, T_α=1 MeV, parabolic density and temperature profiles. The alpha temperature is chosen to be 1 MeV, as it was shown in Refs. [26] and [10] that a slowing-down distribution is well approximated by a 0.5-1 MeV Maxwellian distribution for linear wave-particle interactions, with T_e=25 keV. We see that we study a very wide range of parameters, therefore we present first some general features before going into

details for a given set of parameters. This will enable us to generalize the results and to discuss how they change if ITER parameters are modified.

4.1 Cyclotron frequencies present in the system and range of influence of the α-particles.

In Fig.5, we plot the different cyclotron resonances present in the tokamak in the range considered, 20-90 MHz, with B_0=6T. We see that for $f \geq 65$ MHz, the third harmonic of the tritium is inside the plasma, which makes it impossible to use a model valid up to second-order in Larmor radii, as it is also limited to second harmonics, even to correctly reproduce the dispersion relation.The main scenarii considered in Ref.[25]: 22, 43, 60, 75, and 85 MHz, are also shown and they can be discussed from this figure:

$f \leq 22$ MHz: There are no resonances inside the plasma and only electron heating occurs. This is why f=22 MHz is considered for current drive scenario.

f = 43 MHz: The deuterium fundamental frequency f_D is located in the plasma center and this scenario can be used for ion heating. It was shown in Refs. [11] and [10] that a large fraction of the input power can be absorbed by the alphas instead of the deuterium as they have the same cyclotron frequency. However, it is argued that, in principle, ion heating would no longer be required at the time when α-particle concentration rises significantly, since then α-heating would be the dominant heating source. For this scenario, a detailed parameter study varying n_α/n_e is needed.

f = 60 MHz: The second-harmonic of the alphas is outside the plasma and the fundamental is at the high field side (HFS) of the plasma, therefore the α-particles have little influence if single-pass absorption occurs in the LFS region. In this case, most of the power is absorbed directly by the electrons and some by the tritium species at $2f_T$. If

He^3 is present, then it absorbs more power than the tritium. This scenario is a very good candidate for electron heating and current drive, as the coupling is probably better than for f=22 MHz.

f = 75 MHz: With 1-2% of He^3 or H, ion heating at the q=1 surface is considered for sawtooth and burn control. However, the alpha second-harmonic is near the antenna and might absorb most of the power.

f = 85 MHz: Heating at f_H in the core plasma can be used. However, as $f_H=2f_\alpha$, α-particles may absorb most of the power.

We see from Fig.5 that α-particles should have little influence only for $f \leq 30$ MHz and $50 \leq f \leq 64$ MHz, for B_0=6T. These windows move according to B_0 and become $34 \leq f \leq 43$ MHz for B_0=4T and $f \leq 22$ MHz for B_0=2T in the range of frequencies considered here (20-90 MHz). Thus, for $B_0 \leq 2$T, strong influence of alphas is expected over the whole frequency range. In order to better quantify the range over which α-particles should not contribute, it is worthwhile plotting the minimal value of $|\xi_{n\alpha}|$ vs. x, where $\xi_{n\alpha}= (\omega - n\omega_{c\alpha})/(k_{//} v_{T\alpha})$, that is the value of the argument of the plasma dispersion function for the closest resonance . We know that resonant particles do not absorb much power if $|\xi_n| > 2.5$ [10]. Therefore, we see in Fig.6a that, for B_0=6T, the alphas will have a very strong influence for f≈43 MHz (and 85) and f≈75 MHz near the antenna on the LFS, and some influence for f≈60 MHz if and only if the wave penetrates on the HFS of the plasma cross-section. The curve for f=22MHz does not appear on Fig.6a as $|\xi_{n\alpha}| > 3$. However, if the magnetic field is reduced to 2T, Fig.6b, as is considered for advanced scenarii in ITER, then there are much more resonances present in the plasma. We see that the alphas will have a strong influence throughout the plasma for all frequencies above 22 MHz, when the second harmonic starts to penetrate at the LFS of the plasma. Naturally, the value of $|\xi_{n\alpha}|$ depends strongly on $n_{//}$ and varying it in a plot like Fig.6 gives a precise estimate of the width over which α-particles absorb power.

4.2 Evaluation of the different scenarii considered for B_0=6T.

We study in this Section the influence of α-particles for the different scenarii discussed in Ref.[25]:

f = 22 MHz: As mentioned above, the α-particles do not absorb any power except for $B_0 \leq 2T$. However the coupling and electron single-pass absorption is not very good for such low frequencies. Thus, eventhough the α-particles do not affect this scenario, one should first verify in present tokamaks that enough power can be coupled to the electrons in such a scenario. The first attempts on JET have been inconclusive [27]. Note that for B_0=2T, n_α/n_e=2% and $n_{//}$=9, P_α/P_{tot}=99% for f=22MHz but only 24% for f=20MHz. However, the wave is completly absorbed for x≥0.6m.

f = 43 MHz: The aim of this scenario is to heat the deuterium species in the core plasma. It is maximized in a tritium rich mixture with n_D/n_T=0.3 [25], which is what we have taken for this scenario. As the coupling is maximum for $n_{//} \approx 5$, we have taken this value to obtain the results shown in Fig.7. We see that the power absorbed by the deuterium, P_D, drops rapidly with increasing α-concentration. Already with n_α/n_e=0.5%, P_D drops by about 50%, from 47% to 25% of the total power. Therefore, one can use this scenario for ion heating only if 1% α-concentration is sufficient to replace the RF power. Note that if the effective α-temperature is closer to 0.5MeV, P_D/P_{tot}=30% with n_α/n_e=0.5% and 24% with 1% α-concentration. We also see in Fig.7 that with 0.5% alphas, they are the dominant absorbing species, whereas with T_α=0.5 MeV, they dominate with n_α/n_e=1%. Note also that if one doubles the frequency, f=86-90 MHz, the same effects are obtained.

f = 60 MHz: As mentioned previously, the α-particles do not absorb any power, except for n_α/n_e>10%, as the electrons (67%) and the tritium (33%)

absorb all the input power in $x \geq -0.2$, where $|\xi_{n\alpha}|$ is large. Therefore, for $2 \leq n_{//} \leq 7$ ($2.5 \leq k_{//} \leq 9$) there is a good coupling and strong electron absorption with no effects of α-particles. This is probably the best scenario for electron current-drive and/or tritium heating.

f = 75 MHz: - With $n_{He^3}/n_e = 2\%$, most of the power is absorbed by the deuterium at the second harmonic (98%), at the LFS, and the wave does not reach the He^3 resonance on the HFS. Note that with 1% alphas, P_D/P_{tot} drops to 52%, and with 2% α-particles $P_D/P_{tot} = 33\%$. The wave is completly absorbed in the region $x \geq 1.5$m.

- With $n_H/n_e = 2\%$, all resonances for H, D and α lie at the same x position and the power absorbed by each ion species for different α concentration are given in table 1, the complement being absorbed by the electrons.

n_α/n_e	P_H/P_{tot}	P_D/P_{tot}	P_α/P_{tot}
0%	72%	22%	0
1%	58%	17%	20%
2%	47%	13%	34%
4%	34%	9%	53%

Table 1: Power absorbed by ions with f=75MHz, $n_H/n_e = 2\%$, $n_{//} = 4$ and $B_0 = 6$T.

In this case the input power is also completly absorbed at the cyclotron resonances, for $x \geq 1.5$m. We see that this scenario is probably not suitable for burn control if $n_\alpha/n_e \geq 3\%$. Moreover, it might be delicate to heat the alphas so close to the edge.

f = 85 MHz: As predicted and similarly to the 43 MHz case, the α-particles have a strong influence for this scenario. In this case, second-harmonic heating takes place. Without alphas, with 2% H and $n_{//} = 4$, 40% of the power is absorbed by the hydrogen, 18% by the deuterium and

42% by the electrons. But already with n_α/n_e=0.5%, P_H/P_{tot} drops to 23% and P_D/P_{tot} to 9%, whereas P_α/P_{tot}=26%. With n_α/n_e=1%, these values are equal to 16%, 6%, and 41% respectively. Therefore this scenario is not very useful, especially as the presence of H requires a higher α-concentration [25].

Thus, for B_0=6T, we see that only the scenarii f=22 MHz and f=60 MHz do not suffer by the presence of α-particles, while the other scenarii are strongly modified for n_α/n_e=1-2%.

4.3 Evaluation of the scenarii for B_0=2-6T.

We have discussed in the previous Section the different scenarii using the nominal magnetic field. As it is considered to reduce B_0, for example for advanced tokamak operation and to study steady-state reactor issues, we consider in this Section the scenarii f=22, 43 and 60 MHZ with B_0=2 and 4T. For each frequency and magnetic field, we have taken $n_{//}$=4 and 9. To present the results obtained and the effects of the α-particles, we show two tables, Tables 2 and 3, summarizing the results with no α-particles and with n_α/n_e=2% respectively. If needed, we comment the results with lower or larger α-concentration. The different values in the Tables, for a given B_0 and $n_{//}$, correspond to:

First line: a) the real part of the antenna power, in arbitrary units, enabling one to compare the coupling between different cases; b) P_e/P_{tot}; c) the x-coordinate at the LFS of which all the power is absorbed and indicating if it is central or edge heating;

Second line: P_i/P_{tot} for the ions i which absorb some power.

On top of that, we have filled in dark gray the regions were the coupling is very bad, due for example to a cut-off near the antenna or if the wave does not penetrate further inside than x=2m. We have also highlighted with dots the regions where strong α-particles effects occur.

B_0 [T]	$n_{//}$	22 MHz	43 MHz	60 MHz
6	4	1.3 10^{-4}; 100%; -2.8m	9 10^{-4}; 61%; -0.1m 39%(D)	5 10^{-3}; 66%; -2.3m 1%(D); 33%(T)
	9	2 10^{-4}; 100%; -2.8m	1 10^{-3}; 29%; -0.3m 71%(D)	6 10^{-3}; 64%; -2.2m 7%(D); 29%(T)
4	4	10^{-5}; 100%; 1.8m	1.8 10^{-3}; 88%; -0.7m 12%(T)	3.8 10^{-3}; 89%; 0.0m 10%(D); 1%(T)
	9	10^{-5}; 100%; 1.8m	2 10^{-3}; 82%; -0.7m 18%(T)	1.4 10^{-3}; 81%; 0.0m 18%(D); 1%(T)
2	4	5 10^{-4}; 100%; 1.7m	1.5 10^{-3}; 86%; 1.3m 14%(T)	3.4 10^{-3}; 33%; 1.6m 67%(D)
	9	10^{-3}; 71%; 1.8m 29%(D)	3.3 10^{-3}; 89%; 1.0m 11%(T)	3.4 10^{-3}; 72%; 1.6m 28%(D)

Table 2: D-T scenarii varying B_0 and $n_{//}$ with no α-particles and $n_D=n_T$, except for f=43MHz where $n_D=0.3\ n_T$.

B_0 [T]	$n_{//}$	22 MHz	43 MHz	60 MHz
6	4	1.3 10^{-4}; 100%; -2.8m	1.9 10^{-3}; 26%; -0.3m 7%(D); 67%(α)	4 10^{-3}; 74%; -2.0m 1%(D);22%(T);3%(α)
	9	2 10^{-4}; 100%; -2.8m	1 10^{-3}; 19%; -0.2m 23%(D); 58%(α)	2.5 10^{-4}; 60%; -2.2m 1%(T); 39%(α)
4	4	10^{-5}; 100%; 1.8m	1.8 10^{-3}; 78%; -0.8m 4%(D); 18%(α)	3.8 10^{-3}; 66%; 0.2m 34%(α)
	9	10^{-5}; 100%; 1.8m	2 10^{-3}; 32%; -0.3m 1%(D); 67%(α)	1.4 10^{-3}; 42%; 0.5m 1%(D); 57%(α)
2	4	2.5 10^{-4}; 1%; 2.2m 99%(α)	1.5 10^{-3}; 64%; 1.3m 9%(T); 27%(α)	3.4 10^{-3}; 7%; 2.0m 5%(D); 88%(α)
	9	10^{-3}; 8%; 2.1m 4%(D); 88%(α)	3.3 10^{-3}; 37%; 1.0m 2%(T); 61%(α)	3.4 10^{-3}; 37%; 1.7m 8%(D); 55%(α)

Table 3: Same as Table 2, but with $n_\alpha/n_e=2\%$.

We see that the α-effects are enhanced when the magnetic field is reduced as more α-cyclotron resonances are inside the plasma cross-section or near the LFS boundary, as was shown in Fig.6b. The only set of parameters for which α-effects are small are scenarii corresponding to the f=60MHz, B_0=6T case. Indeed, if one keeps f/B_0=10 MHz/T constant, one stays in between the same resonances and the relative influence of the α-particles remains about the same. Thus the corresponding scenario with 4T, at f=40 (or 43 MHz with small $n_{//}$), is also good and is little influenced by the alphas.

5. Conclusion

We have developed a new gyrokinetic 1D model for the propagation of electromagnetic waves in nonuniform bounded plasma slabs. We have derived a new integral equation in Fourier space valid to all orders in Larmor radii, arbitrary density and anisotropic temperature profiles, assuming Maxwellian distribution functions. We have been able to write this equation in a comprehensive way. Assuming k_y=0, where y is the direction normal to the inhomogeneity and the magnetostatic field B_0, we have derived the equation in configuration space, assuming slowly varying B_0. The equation for the electric field **E** consists of one first-order and two second-order integro-differential equations for E_x and E_y, E_z respectively. We have developed a new code SEMAL [1] which solves these equations, with adequat boundary conditions, using a non-polluting finite element method. We have presented the convergence properties of our code and compared it with the code ISMENE, which solves the same equations but valid up to second order in Larmor radii, to show that SEMAL solves correctly the system of integro-differential equations.

We have used SEMAL to study ICRF scenarii for ITER for a wide range of parameters: f≈20-90 MHz, B_0≈2-6T $n_{//}$≈4-9, n_α/n_e≈0-10%. We have first discussed the main features of the different scenarii considered: f=22, 43, 60, 75, and 85 MHz. Then we have studied in more details the effects of the α-particles with B_0=6T. This shows that only the scenarii f=22MHz and 60MHz are not modified by the presence of α-particles. For the other scenarii, even a

concentration as low as 0.5% reduces by 50% the power absorbed by the ion species. Thus, if more than 1% of alphas is needed to replace the RF heating by α-heating, these scenarii will not work correctly. We have also seen that the coupling between an antenna current located in the vacuum region on the LFS and the plasma is much better for f=60MHz than for 22MHz, as Landau and transit-time magnetic pumping are not very efficient for such a low frequency. Thus the 60MHz scenario with B_0=6T seems to be the best scenario for electron and tritium heating and for current drive.

We have also studied these scenarii with a reduced magnetic field, at 2 and 4 Tesla. This shows again a very strong influence of the α-particles over most of the parameter space and frequency range considered. In fact, only the scenarii with f/B_0=10 MHz/T are little influenced by the α-particles and are good scenarii for reactor-like parameters. This correspond to a frequency such that the second harmonic of the alphas, $2f_\alpha$, is outside the plasma and f_α is on the HFS. Note that with 1-2% of He^3, these scenarii can be used for He^3 heating.

Acknowledgement

We are very grateful to Dr. K. Appert for stimulating discussions and useful suggestions. This work was partly supported by the Swiss National Science Foundation.

References

[1] O. Sauter, Nonlocal analyses of electrostatic and electromagnetic waves in hot, magnetized, nonuniform, bounded plasmas, Swiss Federal Institute of Technology Lausanne, Thesis No. 1000(1992).

[2] M. Brambilla, Comput. Phys. Rep. 4 (1986) 71.

[3] L. Villard, K. Appert, R. Gruber and J. Vaclavik, Comput. Phys. Rep. 4 (1986) 95.

[4] K. Appert, T. Hellsten, J. Vaclavik, L. Villard, Comput. Phys. Commun. 40 (1986) 73, and, K. Appert, T. Hellsten, H. Lütjens, O. Sauter, J. Vaclavik and L. Villard, in Proc. Int. Conf. on Plasma Physics, Kiev, Invited Papers, Ed. A.G. Sitenko (World Scientific, Singapore, 1987) p. 1230.

[5] E.F. Jaeger, D.B. Batchelor and H. Weitzner, Nucl. Fusion 28 (1988) 53.

[6] A. Fukuyama, K. Itoh and S.-I. Itoh, Comput. Phys. Rep. 4 (1986) 137.

[7] D. Edery and H. Pick, Comput. Phys. Commun. 40 (1986) 95, and, D.J. Gambier, A. Samain, Nucl. Fusion 25 (1985) 283.

[8] M. Brambilla, T. Krücken, Nucl. Fusion 28 (1988) 1813.

[9] Th. Martin, J. Vaclavik, Helv. Phys. Acta 60 (1987) 471.

[10] O. Sauter, J. Vaclavik, Nucl. Fusion 32 (1992) 1455.

[11] D. Van Eester, R. Koch, and V. Nys, in Theory of Fusion Plasmas (Proc. Joint Varenna-Lausanne Int. Workshop, Varenna, 1990), Editrice Compositori, Bologna (1990) 339.

[12] O. Sauter, J. Vaclavik, Europhys. Conf. Abstr. **12B**, Part II, (1988) 758; O. Sauter, J. Vaclavik, F. Skiff, Phys. Fluids B **2** (1990) 475.

[13] F. Yasseen, J. Vaclavik, Phys. Fluids 29 (1986) 450.

[14] M. Watanabe, Y. Serizawa, H. Sanuki, T. Watanabe, J. Phys. Soc. Jpn 50 (1981) 1738.

[15] B.D. Fried and S.D. Conte, The plasma dispersion function, Academic, New York, 1961.

[16] R.C. Myer, B.D. Fried, Phys. Fluids B 3 (1991) 2727.

[17] M. Brambilla, Plasma Phys. and Contr. Fusion 33 (1991) 1029.

[18] B.D. McVey, R.S. Sund, J.E. Scharer, Phys. Rev. lett. 55 (1985) 507.

[19] J. Vaclavik, K. Appert, Plasma Phys. & Contr. Fusion 29 (1987) 257.

[20] O. Sauter and J. Vaclavik, in Theory of Fusion Plasmas (Proc. Joint Varenna-Lausanne Int. Workshop, Varenna, 1990), Editrice Compositori, Bologna (1990) 403.

[21] A.B. Mikhailovski, Theory of plasma instabilities, Vol. 1, p. 194, Consultants Bureau, New York (1974).

[22] J. Vaclavik, K. Appert, Nucl. Fusion 31 (1991) 1945.

[23] M. Abramowitz, I.E. Stegun, Handbook of Mathematical Functions, National Bureau of Standards, Washington, DC, 1964.

[24] A. Cardinali , R. Cesario , F. De Marco, O. Sauter, Proc. Europhys. Top. Conf. on RF and Current Drive of Fusion Devices, Brussels 1992, Europhys. Conf. Abstr. **16E**, (1992) 153.

[25] J. Jacquinot, R. Koch, oral presentations at the ITER Technical Meeting on RF heating and Current Drive, Garching, 21-26 October 1993 (private communication).

[26] R. Koch, Phys. Lett. A **157** (1991) 399.

[27] C. Gormezano, and JET team, in Proc. of the 14th Int. Conf. on Plasma Physics and Controlled Nuclear Fusion Research, Würzburg, Germany, 1992 (IAEA Vienna, 1993), Vol.1, p.587.

[28] T. M. Antonsen and W. M. Manheimer, Phys. Fluids 21 (1978) 2295.

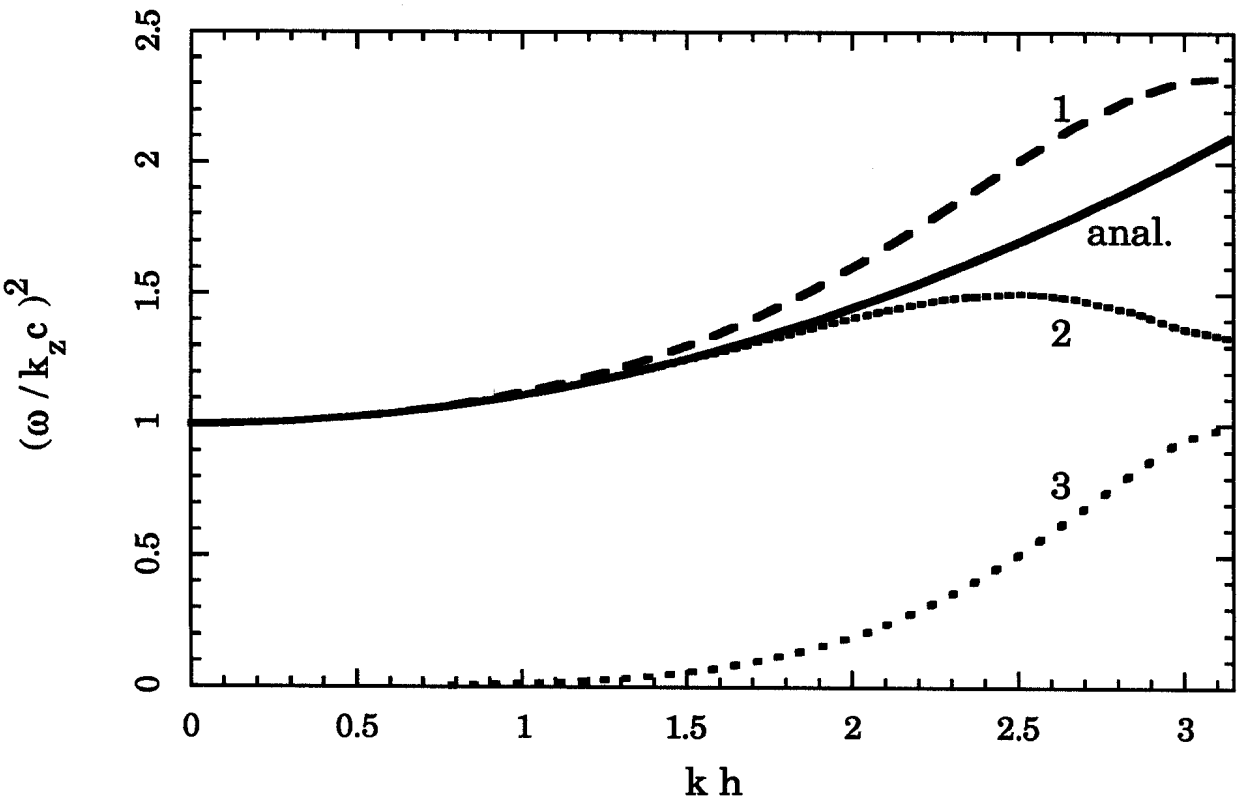

Fig.1: Analytical (solid line) and discretized (curves 1, 2 and 3) dispersion relation. The three dashed curves correspond to the three roots obtained with linear basis functions for E_x, and E_y, E_z. With piece-wise constant and linear basis, respectively, one obtains $\omega=0$ and the root labelled 1 twice degenerated.

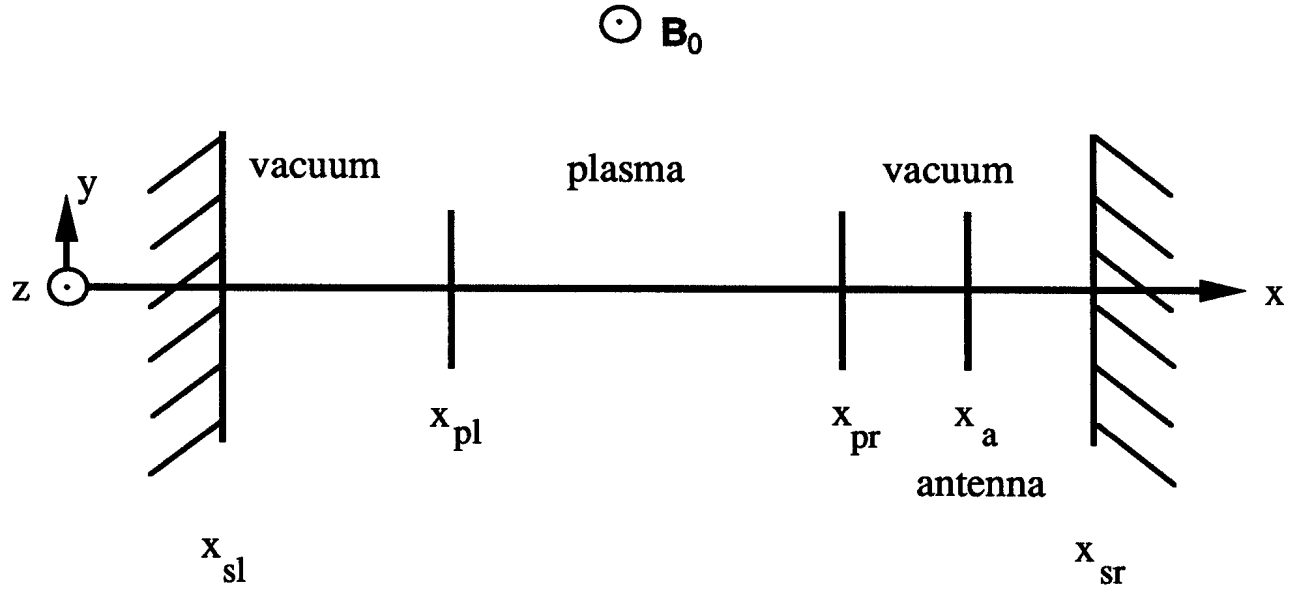

Fig.2: Configuration of the slab model. The plasma is situated between two vacuum regions which are limited by perfectly-conducting walls. An idealized antenna is located in vacuum on the right-hand side of the plasma. The current flows in the (y, z) plane. The equilibrium magnetic field $B_0(x)=B_0R_0/(R_0\pm x)$ is parallel to the z-axis.

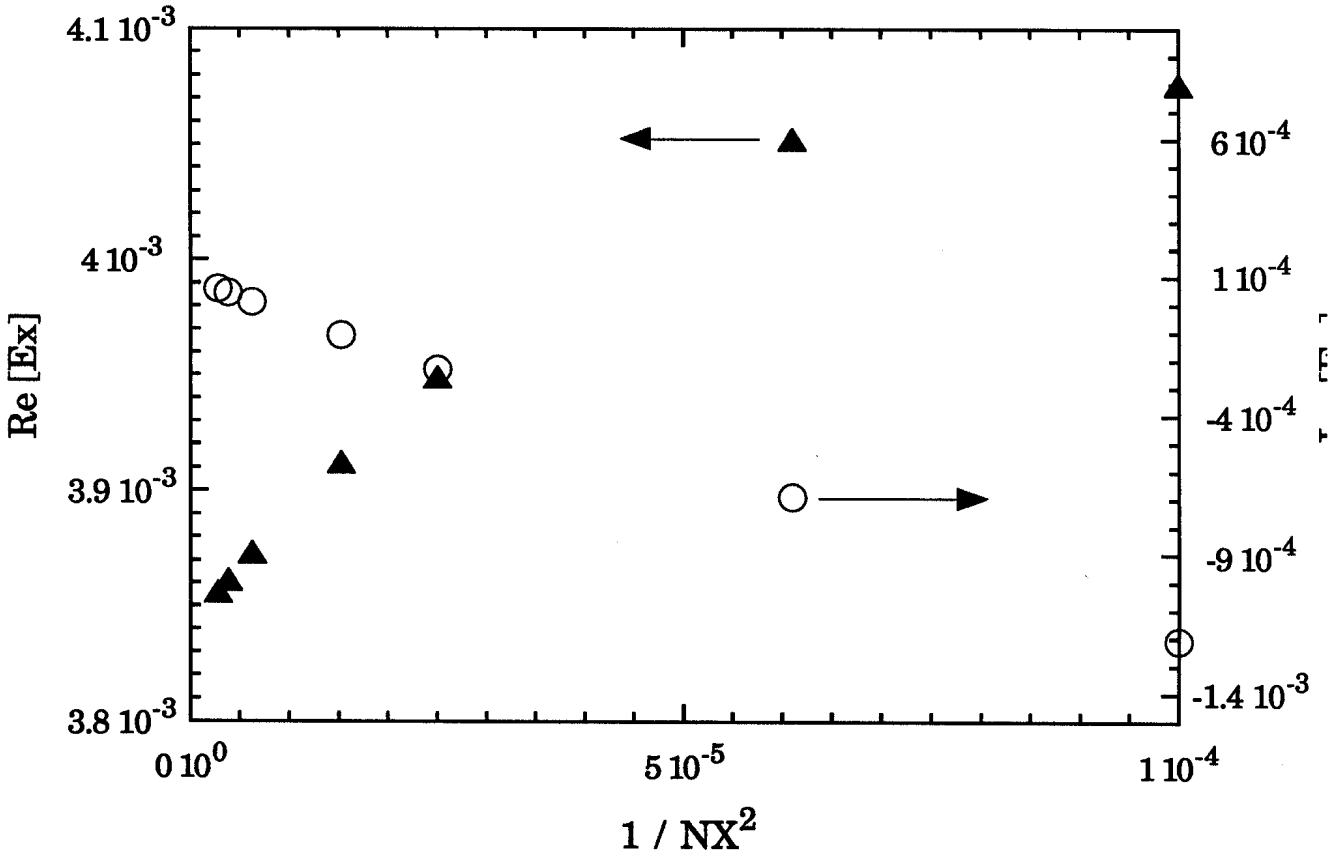

Fig.3: Convergence study for the real (triangles) and imaginary (circles) parts of E_x at the LFS plasma boundary x_{pr}.

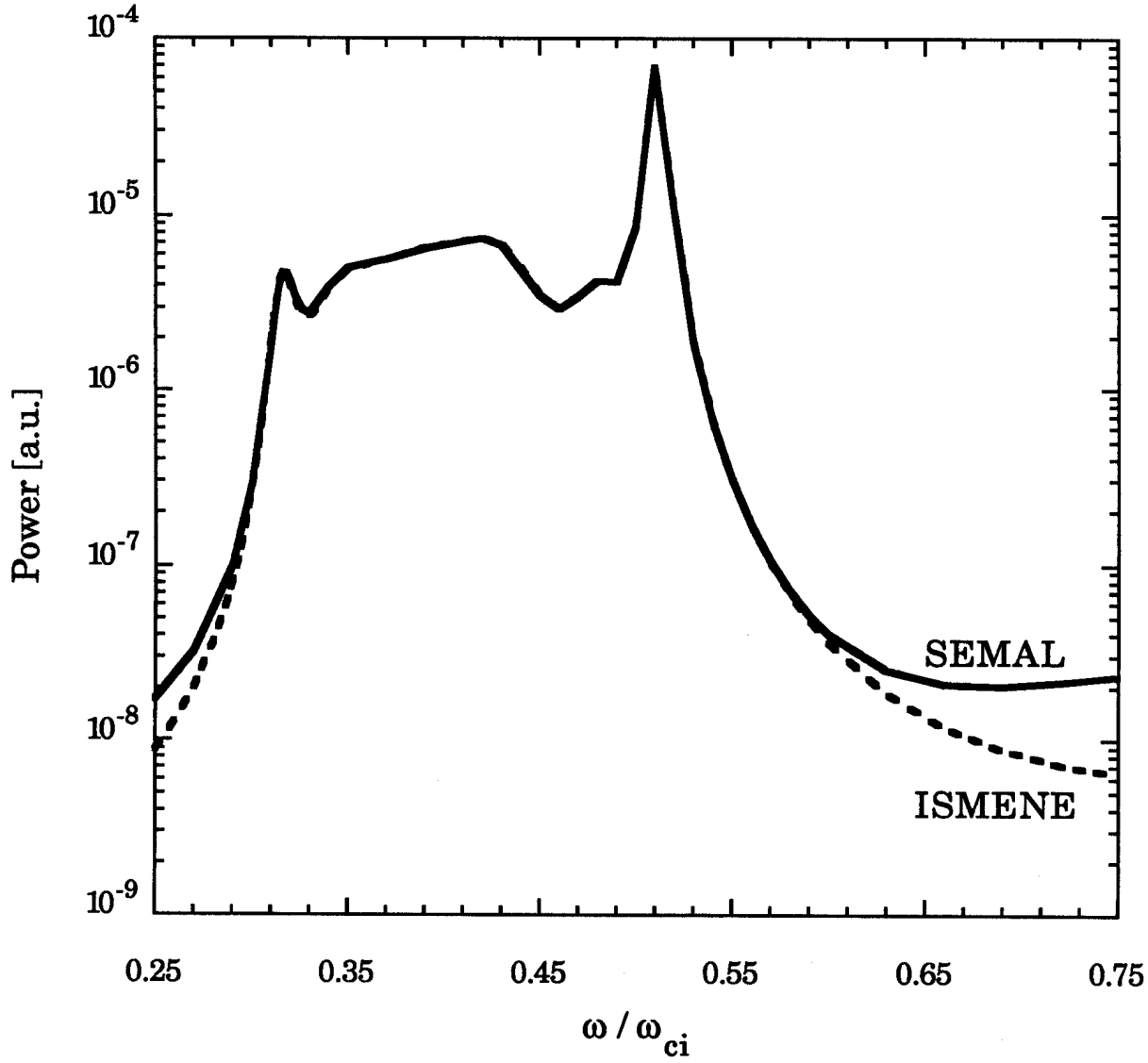

Fig.4: Power emitted by the antenna in the AWRF ($k_{//}\, v_A/\omega_{ci} \approx 0.3$) obtained with SEMAL (solid line) and ISMENE (dashed line), using inhomogeneous temperature and density profiles with very low ion temperature.

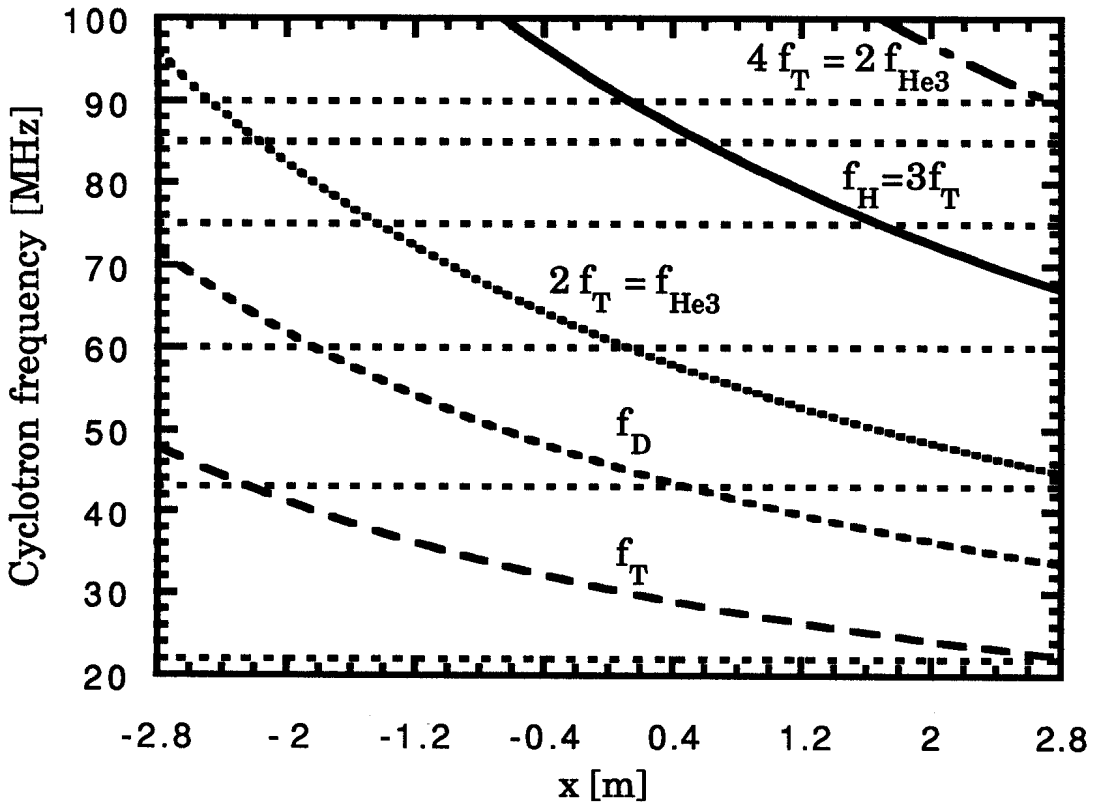

Fig.5: First four cyclotron frequencies present in ITER with R_0=7.7m, a=2.8m, B_0=6T. The horizontal lines correspond to f=22, 43, 60, 75, 85, and 90 MHz.

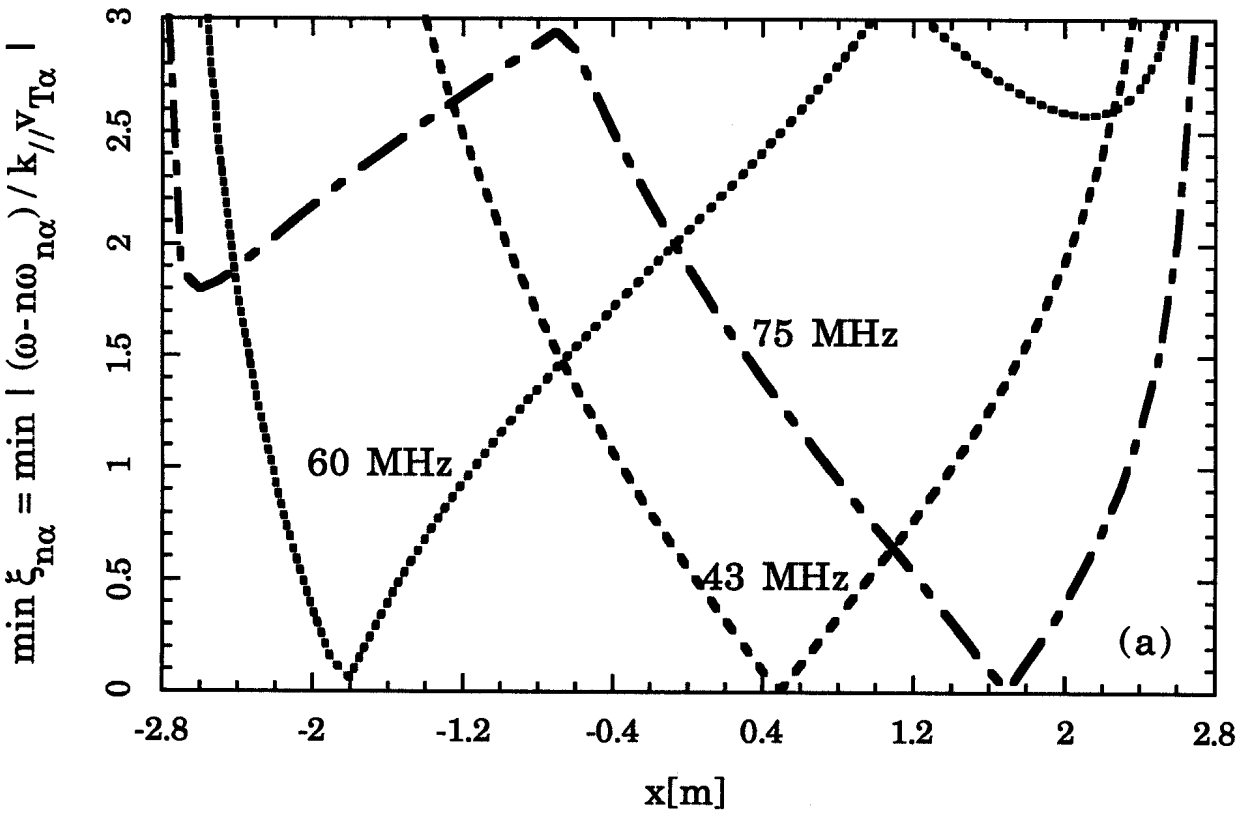

Fig.6a: Smallest argument of plasma dispersion function for alphas with B_0=6T.

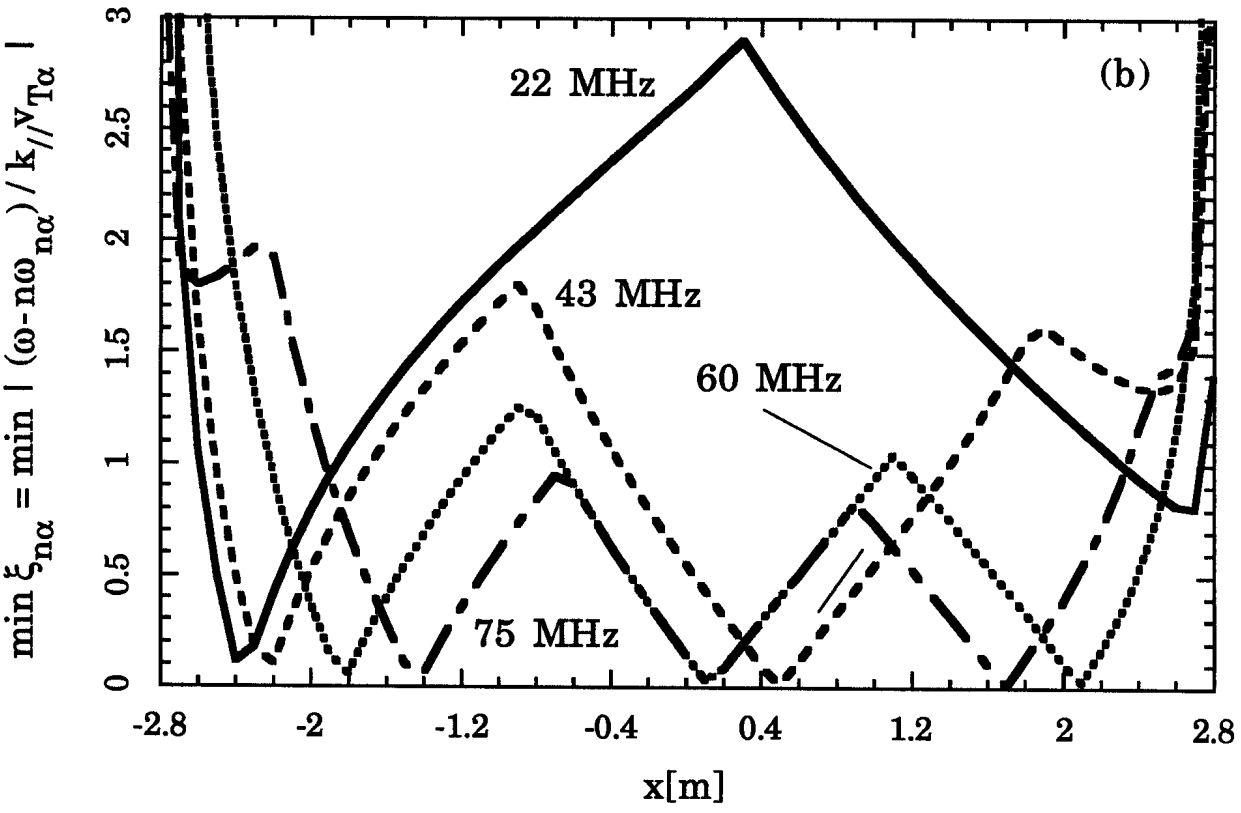

Fig.6b: Same as Fig.6a, but with B_0=2T.

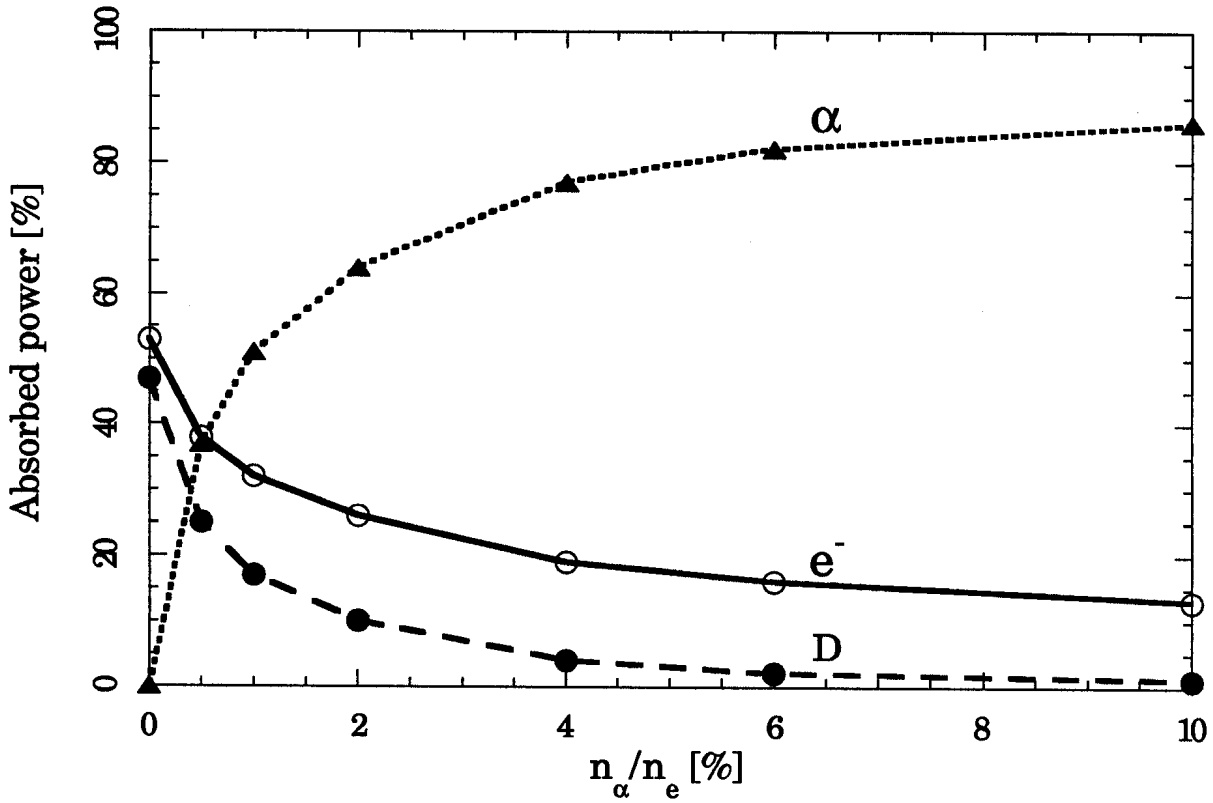

Fig.7: Relative absorbed power vs. α-concentration for each species for f=43 MHz and B_0=6T.